Optimization of Age of Information in Adaptive FD/HD Cooperative SWIPT NOMA/OMA System

Kaboyo, Simon
Electronics and Communications Engineering, Egypt-Japan University of Science and Technology

Abo-Zahhad, Mohammed
Electronics and Communications Engineering, Egypt-Japan University of Science and Technology

Muta, Osamu
Faculty of Information Science and Electrical Engineering, Kyushu University

Abd El-Malek, Ahmed H.
Electronics and Communications Engineering, Egypt-Japan University of Science and Technology

他

出版情報：IEEE Access, 2025-08-13. Institute of Electrical and Electronics Engineers (IEEE)
バージョン：

IEEE Access
Multidisciplinary | Rapid Review | Open Access Journal

Date of publication xxxx 00, 0000, date of current version xxxx 00, 0000.

Digital Object Identifier 10.1109/ACCESS.2017.DOI

Optimization of Age of Information in Adaptive FD/HD Cooperative SWIPT NOMA/OMA System

SIMON KABOYO [1], (Member, IEEE), MOHAMMED ABO-ZAHHAD [1,2], (Senior Member, IEEE), OSAMU MUTA [3], (Member, IEEE), AHMED H. ABD EL-MALEK [1], (Senior Member, IEEE), and MAHA M. ELSABROUTY [1], (Senior Member, IEEE)

[1]Electronics and Communications Engineering, Egypt-Japan University of Science and Technology, New Borg El-Arab City, Alexandria 21934, Egypt
[2]Department of Electrical Engineering, Faculty of Engineering, Assiut University, Assiut 71515, Egypt
[3]Faculty of Information Science and Electrical Engineering, Kyushu University, Fukuoka 812-0053, Japan

Corresponding author: Simon Kaboyo (simon.kaboyo@ejust.edu.eg)

This research was supported in part by JSPS Grants-in-Aid for Scientific Research 24K07490. We also acknowledge financial and technical assistance from the Egypt-Japan University of Science and Technology (E-JUST) and the Egypt Ministry of Higher Education.

ABSTRACT

The Age of Information (AoI) is a key metric in monitoring and control applications of Internet of Things (IoT) networks, where real-time decision-making relies on the freshness of the information. This paper presents an innovative approach to optimizing the AoI in downlink NOMA/OMA systems. We propose an AoI minimization-oriented adaptive framework that selects the optimal transmission mode from four operational strategies: full-duplex (FD) cooperative simultaneous wireless information and power transfer (SWIPT) non-orthogonal multiple access (NOMA), half-duplex (HD) cooperative SWIPT NOMA, regular NOMA, and orthogonal multiple access (OMA). Since the FD cooperative SWIPT NOMA requires the near user to be equipped with two antennas to enable FD operation, we propose enhancing the HD, OMA, and regular NOMA modes of operation by applying beamforming diversity. The proposed work analytically evaluates the system error performance by deriving closed-form expressions of the average block error rate (BLER) for the four operating modes and validates the results through Monte Carlo simulations. Based on the average BLER, the AoI for each operational mode is analysed, illustrating the necessity of the adaptive system. Furthermore, we utilize the finite state Markov decision process to devise an optimal adaptive policy that selects the best transmission strategy based on the AoI in the transmission time slot. Finally, we present a suboptimal policy using the drift-plus-penalty algorithm to reduce system complexity while maintaining near-optimal performance. The results demonstrate that the proposed approach minimizes the AoI, providing valuable insights into system design.

INDEX TERMS Age of Information (AoI), Block error rate (BLER), cooperative NOMA, short-packet communication, full-duplex relaying, half-duplex relaying.

I. INTRODUCTION

The plethora of applications in the 5G and beyond technologies has significantly accelerated communication capabilities for the Internet of Things (IoT). Technologies such as ultra-reliable and low-latency communication (URLLC) are crucial enablers for real-time control, reliable sensing, and edge computing applications in the IoT [1], [2]. Applications such as smart medical systems and industrial automation rely heavily on the timely availability of control and monitoring information, hence requiring metrics to evaluate the performance.

While traditional metrics like throughput and latency play a role, they do not fully capture the essence of real-time and the concept of the freshness of information. The age of information (AoI) emerges as a valuable metric for information freshness without depending on the information source [3]. AoI extends beyond latency by taking into account both the arrival time of the information and the duration since the last update [4]. Several factors influence the AoI, as detailed in the literature, including the packet arrival rate at the source

TABLE 1. A Comparative Analysis of this Work and Prior Studies on Multiple Access Schemes in AoI Systems

Reference	Multiple access schemes			Antenna diversity			Relaying		Beamforming	Optimization	
	OMA	NOMA	SWIPT NOMA	SISO	SIMO	MISO	HD	FD		Optimal Policy	Sub Optimal
A Maatouk, et al [8].	✓	✓	✗	✓	✗	✗	✗	✗	✗	-	-
Q.Wang et al [10].	✓	✓	✗	✓	✗	✗	✗	✗	✗	MDP	Max weight
Shaohua et al [11].	✓	✓	✓	✓	✗	✗	✓	✗	✗	MDP	Lyapunov
Kaboyo et al [12].	✓	✓	✓	✓	✗	✗	✗	✓	✗	-	-
This work	✓	✓	✓	✓	✓	✓	✓	✓	✓	MDP	DPP

nodes [5], the scheduling methods for the transmission [6], the queuing techniques employed [7], and the access scheme used in the network [8].

In IoT systems, the transmitted information is often in the form of short bursts with finite block lengths (FBL), leading to the prevalence of short packet communication (SPC). Consequently, the authors of [9] established a foundation for the study of SPC by analyzing the achievable rate and outage probability in terms of the average block error rate (BLER). Additionally, the adopted cellular access methodologies, such as orthogonal multiple access (OMA) and non-orthogonal multiple access (NOMA), coupled with strategies such as energy harvesting (EH), simultaneous wireless information and power transfer (SWIPT), and cooperative communication, substantially influence the information timeliness within wireless networks. SWIPT offers a solution to energy constraints in battery-powered devices, making it integral to AoI analysis in communication systems.

A. RELATED WORKS

The average AoI was derived in closed form by applying stochastic hybrid systems [8]. Specifically, the potential of NOMA in reducing the average AoI to support machine-type communication (MTC) is investigated. The study shows that, despite NOMA's superior spectral efficiency over the OMA scheme, a lower AoI is not always guaranteed. Motivated by these findings, a hybrid OMA/NOMA scheme for a two-client scenario was proposed in [10]. The base station (BS) adaptively switches between OMA and NOMA to minimize the AoI of the network. Assuming time-slotted interactions between the BS and clients, the weighted sum is minimized by formulating a Markov Decision Process (MDP) to derive the optimal policy. To reduce complexity, a sub-optimal policy based on the max-weight principle is proposed, offering near-optimal performance.

In [13], the authors introduced a cooperative NOMA transmission scheme that utilizes prior information from the users with better channel conditions. Their results demonstrated that this approach achieved maximum diversity gain for both users. Additionally, [14] investigated SWIPT in NOMA systems and demonstrated that it preserves NOMA's diversity. Building on this, [11] proposed a cooperative SWIPT-NOMA strategy for AoI analysis. Specifically, an adaptive NOMA /OMA /cooperative SWIPT NOMA transmission scheme was proposed since the different transmission schemes outperform each other on different system configurations. The results show that the HD cooperative scheme necessitates a strategic deployment, as two time slots are used to complete the transmission, which increases AoI while reducing the average BLER. Therefore, identifying the optimal operating region is crucial for balancing these trade-offs. To minimize AoI, an adaptive scheme was proposed that leverages all transmission modes using an MDP-based optimal policy and a lower-complexity Lyapunov-based sub-optimal policy. However, a full-duplex (FD) scheme is not considered.

FD strategies have been studied, with error performance in FD cooperative NOMA analyzed in [15] and [16]. To enhance AoI, we proposed an FD cooperative SWIPT-NOMA scheme in [12], achieving superior performance when the near user is within the effective region.

While [11] introduces an adaptive strategy for OMA, NOMA, and cooperative SWIPT NOMA systems, it does not consider FD operation. On the other hand, [12] investigates the AoI performance under FD mode but lacks any adaptive optimization framework. Moreover, the HD-based, OMA, and NOMA baseline modes used in the baseline comparisons do not fully utilize the potential degrees of freedom offered by the two antennas required for FD operation, leaving one antenna idle in other modes. In contrast, this work addresses these limitations by focusing on AoI minimization in cooperative SWIPT-NOMA systems through the incorporation of antenna diversity and cooperative beamforming. These enhancements are integrated into OMA, NOMA, and HD cooperative SWIPT-NOMA modes to fully utilize system capabilities in all operating modes. Table 1 provides a comparative summary of the literature.

B. MOTIVATIONS AND CONTRIBUTIONS

From the previously presented literature review, it can be seen that the full realm of FD cooperative NOMA is not explored as a transmission policy that can minimize the AoI. In our previous work [12], we introduced and analyzed the FD cooperative SWIPT NOMA system. Nevertheless, a closer examination of the system model reveals an unexplored degree of freedom, namely, having the cooperating near user equipped with more than one antenna to enable the FD mode. This extra hardware opens the door for improvement in the FD mode and the HD modes of operation. As such, we further investigate the AoI performance in an adaptive FD/HD cooperative SWIPT NOMA, NOMA, and OMA system. While

not operating in FD mode, we utilize both antennas on UE_1 by introducing the idea of antenna diversity. Additionally, in the HD cooperative phase transmission, the idea of transmit beamforming is introduced, fully utilizing both antennas in this mode. We model the system as a finite state decision problem by defining the maximum AoI and analyzing transitions based on system error performance, quantified by the average BLER. Consequently, we fulfil the Markovian property by analysing the AoI evolution and hence leverage the MDP for optimization. This work's contributions are summarized below.

- We develop a downlink SWIPT NOMA/OMA system model that can operate in FD energy harvesting mode and opportunistically benefit from the mounted antennas to aid the different HD modes through different diversity techniques.
- We derive closed-form expressions for the average BLER at UE_1 under four transmission modes, incorporating maximal ratio combining (MRC) and energy harvesting (EH) for OMA, NOMA, and HD cooperative SWIPT-NOMA schemes. The analytical results are validated through Monte Carlo simulations.
- In the HD scheme, we derive the average BLER at UE2 for the two-phase communication, accounting for EH, receiver diversity at UE1 in the direct phase, and transmit beamforming (BF) from UE_1 to UE_2 in the cooperative phase. The overall average BLER at UE2 is evaluated by combining the direct signal from the base station (BS) and the cooperative signal fromUE_1 using MRC then validated through Monte Carlo simulations.
- Additionally, the AoI for the different transmission schemes is analysed based on their average BLER, demonstrating that the schemes outperform each other depending on the specific system configurations, such as the effective regions in terms of distances.
- Another major contribution is the proposed adaptive OMA, NOMA, and FD/HD cooperative SWIPT NOMA scheme, which selects the best scheme by formulating an MDP to obtain an optimal adaptive scheme.
- Finally, to lower the system's computation complexity, a drift plus penalty (DPP) algorithm is proposed based on Lyapunov optimization that achieves near-optimal performance.

The paper is structured as follows: Section II presents the system model, Section III derives the average BLER, and Section IV analyses AoI performance. Section V presents simulation results, and Section VI concludes the study.

Notations: Bold symbols (e.g., $\mathbf{X}$) represent vector. The Frobenius norm is denoted by $\|\bullet\|$, while $(\bullet)^T$ and $(\bullet)^H$ denote the normal and Hermitian transpose, respectively. Mathematical functions utilized include the probability density function (PDF), $f_X(x)$, of X, the cumulative distribution function (CDF), $F_X(x)$, of X, the Gaussian Q-function $Q(y)$ [17, Eq. 8.25] of y, the gamma function $\Gamma(a)$ of a [17, Eq. 8.31], the lower incomplete Gamma function $\gamma(c, x)$ [17, Eq. 8.35], and the exponential integral function E_i [17, Eq. 8.21].

.

II. SYSTEM MODEL

A. NETWORK MODEL

We consider a downlink FD/HD cooperative SWIPT NOMA/OMA system as illustrated in Fig. 1. The system consists of a base station (BS) that serves a group of two users: UE_1, a nearby user at distance d_1 from the BS, and UE_2, a far user at distance d_2 from the BS. The system integrates the concepts of multi-user decode-and-forward relay systems, as proposed for future IoT networks in [18], with cooperative SWIPT NOMA/OMA as discussed in [11]. UE_1 is equipped with two antennas to enable FD cooperative relaying during the cooperative phase, utilizing energy harvested from the BS during the direct phase. Our model extends existing adaptive strategies by incorporating FD operation and enhances HD schemes through antenna diversity and cooperative beamforming, introducing additional degrees of freedom for improved system performance. The more hardware-enabled UE_1 applies SWIPT on the receiving side, as a portion of the received signal is used for NOMA information decoding and another portion as pure power to be harvested. The power harvested in the initial phase is used to forward the UE_2 signal that is lagged by 1 time slot. The BS dedicates one antenna for the sector that contains the NOMA users, while the far user UE_2 is equipped with one antenna. The system can be efficiently extended to multi-user scenarios by applying NOMA user grouping with parallel processing, as demonstrated in [19]. Consequently, the system model supports four operational modes: FD cooperative SWIPT NOMA, HD cooperative SWIPT NOMA, regular NOMA, and OMA. This analysis focuses on a two-user scenario to ensure analytical tractability while capturing key FD/HD performance insights. Extending to a multi-user case would enhance the model's scalability but introduce challenges such as multi-user interference, resource allocation, and user fairness, further complicating optimization and error performance analysis. The two-user NOMA scenario sufficiently captures key transmission characteristics, as shown in [20]. Extending to multi-user cases to address scalability is left for future work.

B. WIRELESS CHANNEL MODEL

We assume quasi-static, independent and identically distributed (i.i.d) Rayleigh fading channels $h_i \sim \mathcal{CN}(0,1)$ to model small-scale fading and a distance-dependent path loss to model large-scale fading at a rate $d_i^{-\phi}$, where ϕ is the path loss exponent. We further assume zero mean, unit variance additive white Gaussian noise (AWGN) across all the links $\mathrm{BS} \rightarrow \mathrm{UE}_1$, $\mathrm{BS} \rightarrow \mathrm{UE}_2$, $\mathrm{UE}_1 \rightarrow \mathrm{UE}_2$, the residual self-interference (RSI) link, $\mathrm{UE}_1 \rightarrow \mathrm{UE}_1$ for the FD scheme after active interference cancellation. Similar to [21], we assume that the receiver has perfect channel state information (CSI), meaning it has complete and accurate knowledge of the fading process h_i. This assumption is

based on the idea that CSI can be obtained by transmitting known training symbols, which the receiver uses to estimate h_i accurately. The CSI is necessary at UE_2 to enable the construction of the beamforming vector in the cooperative transmission. Therefore, the results provide an upper bound on error performance, serving as a baseline for system design. Therefore, the imperfect CSI scenario is left for future work as well.

C. SIGNAL TRANSMISSION

To facilitate URLLC and mMTC communication, we consider an SPC system as follows. In a given timeslot k, the BS transmits a message to either UE_1 or UE_2 for the OMA mode, contrasting with NOMA where the BS transmits a superimposed message to both users simultaneously [22]. For the cooperative HD and FD relaying modes, the BS transmits simultaneously to the UEs in the direct phase, while in the cooperative phase, UE_1 employs the decode-and-forward (DF) strategy to transmit UE_2's message obtained after successive interference cancellation (SIC) using the harvested energy from the direct phase. Both phases are completed within the same timeslot in the FD scheme, whereas they require two timeslots in the HD scheme [23].

For the NOMA based modes, the BS transmits a superposed signal $x[k] = \sqrt{\alpha_1}x_1[k] + \sqrt{\alpha_2}x_2[k]$ to UE_1 and UE_2 simultaneously using NOMA principle, where α_1 and α_2 are NOMA power allocation coefficients for UE_1 and UE_2 respectively. During the cooperative transmission phase of the, FD/HD cooperative SWIPT NOMA mode, UE_1 transmits the signal $s[k] = \hat{x}_2[k-\tau]$ to UE_2, where τ signifies processing delay, set to 1 [23]. To guarantee the success of MRC at UE_2 for the direct signal from the BS and cooperative phase signal from UE_1, we assume time synchronization be perfect (the receiver knows the signal propagation delay from the transmitting antenna to the receiving antenna)

1) UE_1 signal Transmission for the FD Mode

In the FD mode at UE_1, one antenna is used as a receive antenna while the other is used as a transmit antenna, leading to self-interference w_r. Therefore, the received signal at UE_1 in time slot k is given by [24].

$$y_1^{\mathrm{FD}}[k] = \underbrace{\sqrt{\frac{(1-b)P}{d_1^{\phi}}}h_1 x[k]}_{\text{desired signal}} + \underbrace{\sqrt{P_r}w_r s[k]}_{\text{self interference}} + \underbrace{\mathrm{w}_1[k]}_{\text{AWGN noise}}, \tag{1}$$

where $(1-b)$ is the fraction of the received signal power P utilized for information decoding, h_i is the channel coefficient, and P_r is the average power at UE_1.

We further adopt the self-interference cancellation approach in this mode, utilized in [25], and express the system analysis in terms of the transmit SNR.

$$\rho_r = \frac{{\rho_h}^{(1-\kappa)}}{\psi\mu^{\kappa}}, \tag{2}$$

$$\rho_h = |h_1|^2\rho, \tag{3}$$

where $\rho = \frac{P}{\sigma^2}$ is transmit signal to noise ratio (SNR) at UE_1, parameters κ and μ are dependent on the specific self-interference cancellation approach, and ψ originates from the passive cancellation.

Using SIC, UE_1 decodes x_2 while treating x_1 as interference. Therefore, the signal-to-interference-plus-noise ratio (SINR) of decoding x_2 at UE_1 is given by

$$\gamma_{1,2}^{\mathrm{FD}} = \frac{\alpha_2(1-b)\rho|h_1|^2}{\alpha_1(1-b)\rho|h_1|^2 + \rho_r|w_r|^2 + d_1^{\phi}}, \tag{4}$$

where $\rho = \frac{P}{\sigma^2}$ is the transmit SNR at the BS, and $\mathbb{E}\{x_1^2\} = \mathbb{E}\{x_2^2\} = 1$.

If the SIC is successful, the SINR to detect x_1 at UE_1 is given by

$$\gamma_{1,1}^{\mathrm{FD}} = \frac{\alpha_1(1-b)\rho|h_1|^2}{\rho_r|w_r|^2 + d_1^{\phi}}. \tag{5}$$

2) UE_1 Signal Transmission for the HD Mode

In the HD mode, UE_1 utilises two antennas for information decoding and EH, combining the received signal coherently through MRC in the direct phase (BS to UE_1) and transmit BF in the cooperative phase (UE_1 to UE_2). Therefore, the received signal at UE_1 in time slot k is given by

$$y_1^{\mathrm{HD}}[k] = \sqrt{\frac{(1-b)P}{d_1^{\phi}}}\mathbf{g}_1^H\mathbf{h}_1 x[k] + w_1[k], \tag{6}$$

where $\mathbf{g}_1 \in \mathbb{C}^{N_R * 1}$ is the receive BF vector at UE_1, and N_R number of antennas at UE_1, $(.)^H$ is the Hermitian transpose. By employing MRC, a normalised BF vector is employed by UE_1 as follows [26].

$$\mathbf{g}_1 = \frac{{\mathbf{h}_1}^H}{||\mathbf{h}_1||}, \tag{7}$$

where $\|.\|$ is the Euclidean norm.

UE_1 utilizes SIC to decode x_2 and treats x_1 as interference, then the signals from both receive antennas are combined coherently using MRC to obtain the received SINR of decoding x_2 at UE_1 given by

$$\gamma_{1,2}^{\mathrm{HD}} = \frac{\alpha_2(1-b)\rho(||\mathbf{h}_1||^2)}{\alpha_1(1-b)\rho(||\mathbf{h}_1||^2) + d_1^{\phi}}. \tag{8}$$

After SIC, UE_1 obtains its signal by subtracting the above component from the received signal. Therefore the SNR of detecting x_1 at UE_1 given by

$$\gamma_{1,1}^{\mathrm{HD}} = \frac{\alpha_1(1-b)\rho(||\mathbf{h}_1||^2)}{d_1^{\phi}}. \tag{9}$$

3) UE_1 Signal Transmission for the NOMA and OMA Modes

Similarly, UE_1 utilises both antennas for the reception of in the NOMA mode. Therefore, the observation at UE_1 for

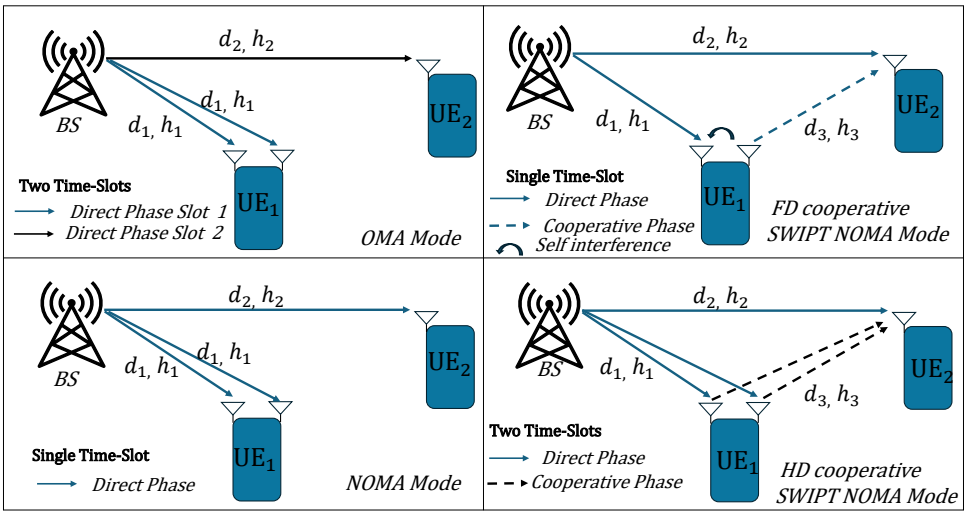

FIGURE 1. The system model illustrating the four transmission modes

NOMA given by

$$y_1^{\mathrm{N}}[k] = \sqrt{\frac{P}{d_1^{\phi}}}\mathbf{g}_1^H \mathbf{h}_1 x[k] + \mathrm{w}_1[k]. \tag{10}$$

Therefore, the received SINRs to detect x_2, and x_1 at UE_1 after SIC are given by

$$\gamma_{1,2}^{\mathrm{N}} = \frac{\alpha_2 \rho ||\mathbf{h}_1||^2}{\alpha_1 \rho ||\mathbf{h}_1||^2 + d_1^{\phi}}. \tag{11}$$

and

$$\gamma_{1,1}^{\mathrm{N}} = \frac{\alpha_1 \rho ||\mathbf{h}_1||^2}{d_1^{\phi}}. \tag{12}$$

Since OMA serves one user at a time, the observation at UE_1 for OMA is given by

$$y_1^{\mathrm{O}}[k] = \sqrt{\frac{P}{d_1^{\phi}}}\mathbf{g}_1^H \mathbf{h}_1 x_1[k] + \mathrm{w}_1[k]. \tag{13}$$

Hence, the received SNR to decode x_1 at UE_1 is given by

$$\gamma_1^{\mathrm{O}} = \frac{\rho ||\mathbf{h}_1||^2}{d_1^{\phi}}. \tag{14}$$

4) UE_2 Signal Transmission for the FD Mode

For the FD mode, UE_2 combines the direct phase signal $x[k]$, and the cooperative phase signal $s[k]$.Therefore, the received signal at UE_2 after the two phases is given by

$$y_2^{\mathrm{FD}}[k] = \sqrt{\frac{P}{d_2^{\phi}}} h_2 x[k] + \sqrt{\frac{P_r}{d_3^{\phi}}} h_3 s[k] + \mathrm{w}_2[k], \tag{15}$$

where h_2 and h_3 are the channel coefficients between BS to UE_2, and UE_1 to UE_2 respectively. The SINR for decoding x_2 at UE_2 is given by

$$\gamma_{2,3}^{\mathrm{FD}} = \gamma_{2,2} + \gamma_{2,1} = \underbrace{\frac{\alpha_2 \rho |h_2|^2}{\alpha_1 \rho |h_2|^2 + d_2^{\phi}}}_{\text{direct phase}} + \underbrace{\frac{\eta b \rho_r |h_3|^2}{d_3^{\phi}}}_{\text{cooperative phase}}, \tag{16}$$

where η is the RF to DC power conversion efficiency.

5) UE_2 Signal Transmission for the HD Mode

In the HD mode, the transmission strategy adopted at UE_1 in the cooperative phase is maximum ratio transmission (MRT) since it is the optimal BF for a single user scenario [27]. BF consists of a channel vector h_3 and the BF vector $\mathbf{g}_3 = \frac{\mathbf{h}_3^H}{||\mathbf{h}_3||}$. Similar to the FD mode, UE_2 combines the signal $x[k]$, and $s[k]$. Therefore, the received signal at UE_2 after the two phases is given by

$$y_2^{\mathrm{HD}}[k] = \sqrt{\frac{P}{d_2^{\phi}}} h_2 x[k] + \sqrt{\frac{P_r}{d_3^{\phi}}} \mathbf{h}_3 \mathbf{g}_3 s[k] + \mathrm{w}_2[k]. \tag{17}$$

The SINR for decoding x_2 at UE_2 is given by

$$\gamma_{2,3}^{\mathrm{HD}} = \gamma_{2,2} + \gamma_{2,1} = \underbrace{\frac{\alpha_2 \rho |h_2|^2}{\alpha_1 \rho |h_2|^2 + d_2^{\phi}}}_{\text{direct phase}} + \underbrace{\frac{\eta b \rho_h ||\mathbf{h}_3||^2}{d_3^{\phi}}}_{\text{cooperative phase}}, \tag{18}$$

where $\rho_h = ||\mathbf{h}_1||^2 \rho$.

6) UE_2 Signal Transmission for the NOMA and OMA Modes

In the NOMA mode, UE_2 receives signal $x[k]$ from the BS. Therefore, the observation at UE_2 is given by

$$y_2^{\mathrm{N}}[k] = \sqrt{\frac{P}{d_2^{\phi}}} h_2 x[k] + \mathrm{w}_2[k]. \tag{19}$$

The received SINR to detect x_2 at UE_2 is given by

$$\gamma_{2,2}^{\mathrm{N}} = \frac{\alpha_2 \rho |h_2|^2}{\alpha_1 \rho |h_2|^2 + d_2^{\phi}}, \tag{20}$$

Since OMA serves one user at a time, the observation at UE_2 is given by

$$y_2^{\mathrm{O}}[k] = \sqrt{\frac{P}{d_2^{\phi}}} h_2 x_2[k] + \mathrm{w}_2[k]. \tag{21}$$

Hence, the received SNR to decode x_2 at UE_2 is given by

$$\gamma_2^{\mathrm{O}} = \frac{\rho |h_2|^2}{d_2^{\phi}}. \tag{22}$$

III. AVERAGE BLER ANALYSIS

The instantaneous BLER for a given SINR $\gamma_{i,j}$ in FBL, SPC, with block length $m \geq 100$ and N bits, is given by [9]

$$\varepsilon_{i,j} \approx \Psi(\gamma_{i,j}, N, m) = Q\left(\frac{C((\gamma_{i,j}) - N/m)}{\sqrt{V(\gamma_{i,j})/m}}\right), \tag{23}$$

where $C(\gamma_{i,j}) = \log_2(1+\gamma_{i,j})$ is the Shannon-capacity, and $V(\gamma_{i,j}) = (1-(1+\gamma_{i,j})^{-2})(\log_2 e)^2$ is the channel dispersion. For fading channels the average BLER $\overline{\varepsilon}_{i,j}$ is given by

$$\overline{\varepsilon}_{i,j} = \mathbb{E}[\varepsilon_{i,j}] \approx \int_0^{\infty} Q\left(\frac{C((x) - N/m)}{\sqrt{V(x)/m}}\right) f_{\gamma_{i,j}}(x)\, dx. \tag{24}$$

Obtaining a closed-form expression for (24) is challenging because of the Q-function's complexity. Therefore, the following linear approximation of the Q-function can be utilized [28].

$$\Psi(\gamma_{i,j}, N, m) \approx Z(\gamma_{i,j}) = \begin{cases} 1, & \gamma_{i,j} \leq v, \\ \frac{1}{2} - \omega(\gamma_{i,j} - \Omega), & v \leq \gamma_{i,j} \leq u, \\ 0, & \gamma_{i,j} \geq u, \end{cases} \tag{25}$$

where $\omega = \frac{\sqrt{m}}{\sqrt{2\pi(2^{2\frac{N}{m}}-1)}}$, $\Omega = 2^{\frac{N}{m}} - 1$, $v = \Omega - \frac{1}{2\omega}$, $u = \Omega + \frac{1}{2\omega}$. By plugging (25) into (24), the average BLER can be rewritten as

$$\overline{\varepsilon}_{i,j} \approx \int_0^{\infty} Z(\gamma_{i,j}) f_{\gamma_{i,j}}(x)\, dx = \omega \int_v^u F_{\gamma_{i,j}}(x)\, dx. \tag{26}$$

Proof: See Appendix A

Since $u - v = \frac{1}{w}$ is generally small for SPC, $\overline{\varepsilon}_{i,j}$ is simplified using first-order Riemann integral approximation as follows [29].

$$\overline{\varepsilon}_{i,j} \approx w(u-v) F_{\gamma_{i,j}} \frac{(u+v)}{2} \approx F_{\gamma_{i,j}}(\Omega). \tag{27}$$

Therefore, the average BLERs at UE_1 and UE_2 are approximated by the associated CDFs at the respective SINR.

A. AVERAGE BLER AT UE_1

For the three NOMA modes, the overall average BLER of decoding $x[k]$ at UE_1 depends on the two stages of SIC [30].

$$\overline{\varepsilon}_1 = \overline{\varepsilon}_{1,2} + (1 - \overline{\varepsilon}_{1,2})\overline{\varepsilon}_{1,1}. \tag{28}$$

Since we utilize two receive antennas in the OMA, NOMA, and HD mode at UE_1, the general closed-form of the CDF is modelled as i.i.d. Rayleigh fading across each antenna, modelled by a chi-squared distribution with two degrees of freedom [31, Ch. 7].

$$F_{i,j}^{\mathrm{O,N,HD}}(\Omega) \approx 1 - \exp\left(\frac{-\Omega}{\overline{\gamma}_{i,j}}\right) \sum_{n=0}^{N_R - 1} \frac{1}{n!} \left(\frac{\Omega}{\overline{\gamma}_{i,j}}\right)^n, \forall \Omega \geq 0, \tag{29}$$

where N_R is the number of receive antennas, $\overline{\gamma}_{i,j}$ the average SINR. Therefore, for the NOMA and the HD cooperative SWIPT NOMA modes, the average BLER at UE_1 is obtained by substituting (29) into (28) while for the OMA mode, the average BLER at UE_1 is obtained directly from (29) since the SIC operation is not required.

The CDF for the FD mode is derived in [23] and extended for SWIPT [12] as follows.

$$F_{1,1}^{\mathrm{FD}}(\Omega) \approx 1 - \frac{\tau_2 \tau_1}{\tau_2 \tau_1 + \Omega} e^{-\Theta\Omega}, \quad \Omega \geq 0, \tag{30}$$

and

$$F_{1,2}^{\mathrm{FD}}(\Omega) = \begin{cases} 1 - \frac{(\chi - \Omega)\tau_2\tau_1}{(\chi-\Omega)\tau_2\tau_1 + \Omega} e^{-\frac{\Theta\Omega}{\chi - \Omega}}, & 0 \leq \Omega \leq \chi, \\ 1, & \omega \geq 0, \end{cases} \tag{31}$$

where $\tau_1 = \frac{1}{\rho_r \lambda_r}$, $\lambda_r = \mathbb{E}|w_r|$, $\tau_2 = \alpha_1(1-b)\rho\lambda_1$, $\lambda_i = \mathbb{E}|h_i|$, $\chi = \frac{\alpha_2}{\alpha_1}$, $\Theta = \frac{\lambda_r \rho_r + 1}{\alpha_1(1-b)\rho\lambda_1}$.
Therefore, for the FD mode the average BLER at UE_1 is obtained by substituting (30), and (31) into (28).

B. AVERAGE BLER AT UE_2

The average BLER associated with decoding $x[k]$ for the HD/FD cooperative SWIPT modes at UE_2 utilizing the DF strategy is given by [30]

$$\overline{\varepsilon}_2 = \overline{\varepsilon}_{1,2}\overline{\varepsilon}_{2,2} + (1 - \overline{\varepsilon}_{1,2})\overline{\varepsilon}_{2,3}. \tag{32}$$

where $\overline{\varepsilon}_{2,2}$ is the error of decoding $x_2[k]$ at UE_2, and $\overline{\varepsilon}_{2,3}$ is the error after two phase signal to UE_2 from UE_1. Errors occur when neither UE_1 nor UE_2 can decode $x_2[k]$ and/or when UE_1 can successfully decode $x_2[k]$ but MRC fails.
For the NOMA, FD, and HD modes, the CDF associated with decoding $x_2[k]$ at UE_2 is given by

$$F_{2,2}^{\mathrm{N,HD,FD}}(\Omega) \approx 1 - \exp \frac{-{d_2}^{\phi}\Omega}{\rho(\alpha_2 - \alpha_1\Omega)}. \tag{33}$$

Proof: See Appendix B

Similarly, the CDF associated with decoding $x_2[k]$ at UE_2 for the OMA scheme is obtained as follows.

$$F_2^{\mathrm{O}} \approx 1 - \exp \frac{-{d_2}^{\phi}\Omega}{\rho}. \tag{34}$$

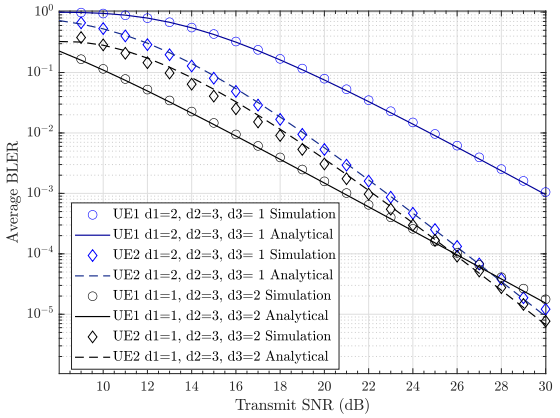

FIGURE 2. Validation of analytical framework of average BLER for the HD cooperative SWIPT NOMA.

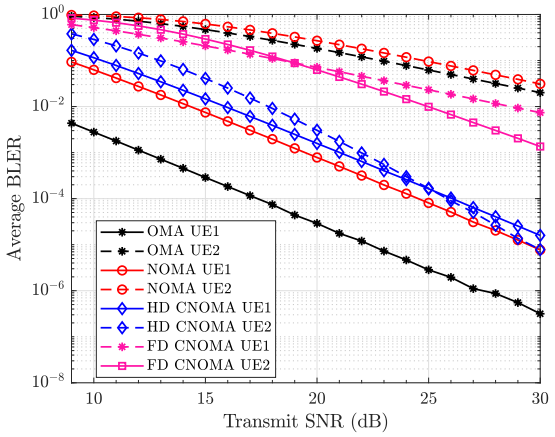

FIGURE 3. Average BLER for each user and mode Vs transmit SNR.

The error $\bar{\varepsilon}_{2,3}$ associated with the two phase communication at UE_2 for the FD cooperative SWIPT NOMA mode is adopted from our previous work [12, Eq. 29].

For the HD cooperative SWIPT mode, we derive $\bar{\varepsilon}_{2,3}$ for the two-phase communication at UE_2 as follows.
Let $X = \frac{\alpha_2\rho|h_2|^2}{\alpha_1\rho|h_2|^2+d_2^{\phi}}$, and $A = \frac{\eta b\rho||\mathbf{h}_1||^2||\mathbf{h}_3||^2}{d_1^{\phi}d_3^{\phi}}$, then

$$F_{2,3}^{\mathrm{HD}}(\Omega) = \mathrm{P_r}\{A + X \leq \Omega\} = \int_0^{\Omega} f_X(x)F_A(a)|_0^{\Omega-x}\, dx. \tag{35}$$

Since the product of two independent Rayleigh channels in A is chi-square distributed [31], the CDF is modelled as a product of gamma distributed variables due to BF [32]. We utilize the accurate approximation of the product of generalized Gamma random variables derived in [33] to obtain the CDF. Moreover, using computationally expensive contour integrals associated with modelling the product of Gamma random variables through the Meijer-G function is avoided [34]. Therefore, from [33, Eq. 25] the CDF $F_A^{\mathrm{HD}}(a)$ is obtained as

$$F_A^{\mathrm{HD}}(a) \approx \gamma\left(m_0 + m\kappa - \kappa, m\frac{2m_0}{\Omega_o}\left(\frac{a}{\Pi_{i=1}^{\kappa}\mathrm{d_i}}\right)^{\frac{v}{\kappa}}\right), \tag{36}$$

where the fading figure, $m_0 = 0.6102n + 0.4263$, the scale parameter $\Omega_0 = 0.8808n^{-0.9661} + 1.12$ and $v > 0$ is the shape parameter, $\kappa = 2$) is the number of antennas while $\mathrm{d_i} = d_i^{\phi}$.

By differentiating (33), $f_B(b)$ is obtained. Then plug the result and (36) in to (35) to obtain $\bar{\varepsilon}_{2,3}^{\mathrm{HD}}$ as

$$\bar{\varepsilon}_{2,3}^{\mathrm{HD}} = \int_0^{\Omega} \frac{F_A^{\mathrm{HD}}(\Omega - x)d_2^{\phi}\alpha_2}{\rho(\alpha_2 - \alpha_1 x)^2}\exp\left(-\frac{d_2^{\phi}x}{\rho(\alpha_2 - \alpha_1 x)}\right) dx. \tag{37}$$

Since (37) is mathematically intractable, $\bar{\varepsilon}_{2,3}^{\mathrm{HD}}(\Omega)$ is approximated by Gaussian Chebyshev quadrature (GCQ) summarised as follows $\int_a^b f(x)\, dx = \frac{b-a}{2}\sum_{i=1}^{M} W_i\sqrt{1-x_i^2}f(\hat{x})$, where $W_i = \frac{\pi}{M}$, $x_i = \cos(\frac{(2i-1)\pi}{2M})$, $\hat{x} = \frac{(b-a)x_i}{2} + \frac{(b+a)}{2}$ and M are the quadrature nodes which serve as the complexity trade-off [35]. Therefore,

$$\bar{\varepsilon}_{2,3}^{\mathrm{HD}}(\Omega) \approx \frac{d_2^{\phi}\alpha_2\pi\Omega}{\Gamma(c)M\rho}\sum_{i=1}^{M}\mathrm{D}(\varphi_i), \tag{38}$$

$$\mathrm{D}(\varphi_i) = \frac{\sqrt{1-\varphi_i^2}\gamma\left(m_0 + m\kappa - \kappa, m\frac{2m_0}{\Omega_o}\left(\frac{\Omega(\varphi_i+1)}{2\Pi_{i=1}^{\kappa}\mathrm{d_i}}\right)^{\frac{v}{\kappa}}\right)}{(2\alpha_2 - \alpha_1\Omega(\varphi_i+1))^2} \times \exp\left(\frac{d_2^{\phi}\Omega(\varphi_i+1)}{2\alpha_2 - \alpha_1\Omega(\varphi_i+1)}\right), \tag{39}$$

where $\varphi_i = \cos\left(\frac{2i-1}{2M}\pi\right)$, $c = m_0 + m\kappa - \kappa$ while M is the number of the quadrature nodes for the complexity trade-off.

Therefore, the average BLER at UE_2 is obtained by substituting (29), (33), and (38) into (32) for the derived HD mode average BLER. The FD mode average BLERs are obtained by making a similar substitution into (32), while average BLER for the NOMA and OMA modes directly utilize (33), and (34) respectively.

The derived HD framework above is validated in Fig. 2, with the average BLER for each user and the operating mode shown in Fig. 3. A detailed discussion of these results is provided in Section V.

IV. EWSAOI OF THE TRANSMISSION MODES

The average BLER in Section III quantifies the system's error performance. Based on this, we model the instantaneous AoI in a given time slot and the overall performance over an infinite time horizon through the expected weighted sum of AoI (EWSAoI).

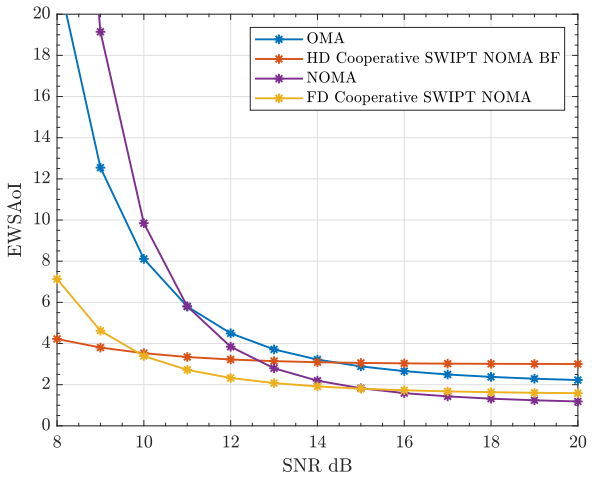

FIGURE 4. Random Policy EWSAoI versus SNR at (d_1=1, d_2=3, d_3=2).

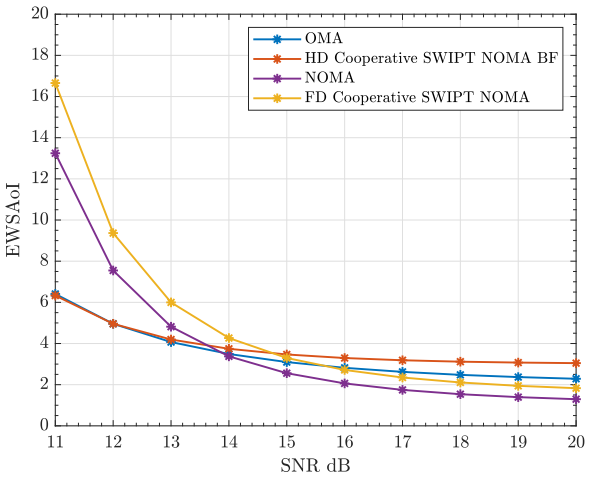

FIGURE 5. Random Policy EWSAoI versus SNR at (d_1=2, d_2=3, d_3=1).

A. AGE OF INFORMATION FORMULATION

From the definition, the AoI of a received packet is [36];

$$\Delta_i = t - G_i(t), \tag{40}$$

where $G_i(t)$ is the generation time of latest packet and t is the arrival time at the destination. The dynamic evolution of the AoI is analysed for the OMA and NOMA schemes as follows. If a user effectively receives a packet within a single time slot, the AoI drops to 1. If not, the AoI increases by 1. The instantaneous AoI, Δ_i, in the next time slot $t+1$ is given by

$$\Delta_i(t+1) = \begin{cases} 1, & \text{if } l_i(t) = 1, \\ \Delta_i(t) + 1, & \text{if } l_i(t) = 0. \end{cases} \tag{41}$$

The variable $l_i(t) \in \{0, 1\}$ is the indicator function that holds a value of 1 when UE_i decodes its packet in the slot t and otherwise equals 0. The BS transmits to one user in one time slot in the OMA mode, while the BS transmits to both users simultaneously if the NOMA mode is selected.

On the other hand, the cooperative modes utilise a two-phase transmission protocol [37]. During the first stage, if UE_1 decodes the packet successfully, the AoI is set to 1. Otherwise, it increases by 1. During this stage, the AoI at UE_2 always increases by 1. The evolution of the AoI is given by

$$\Delta_1(t+1) = \begin{cases} 1, & \text{if } l_1(t) = 1, \\ \Delta_1(t) + 1, & \text{if } l_1(t) = 0, \end{cases} \tag{42}$$

and

$$\Delta_2(t+1) = \Delta_2(t) + 1. \tag{43}$$

During the second phase, UE_2 capitalizes on MRC to combine signals from BS and UE_1 while UE_1 receives the latest update from the BS. The evolution of the AoI is given by

$$\Delta_2(t+1) = \begin{cases} 2, & \text{if } l_2(t) = 1, \\ \Delta_2(t) + 1, & \text{if } l_2(t) = 0. \end{cases} \tag{44}$$

The primary distinction between the HD and the FD cooperative modes is that the HD requires two-time slots to finish the two-phase transmission, whilst the FD strategy only needs one timeslot [38].

To quantify the AoI, we obtain the network wide long-term average through the EWSAoI obtained from the instantaneous AoI (41) through (44) for the respective schemes. The packet delivery $l_i(t)$ is quantified by the average BLER analysed in section III. The EWSAoI is given by

$$\bar{\Delta} = \lim_{T\to\infty} \frac{1}{2T} \mathbb{E}\left[\sum_{t=1}^{T}\sum_{i=1}^{2} w_i \Delta_i\right], \tag{45}$$

where T is the time horizon, $\mathbb{E}[.]$ is the expectation operator, w_i the weight associated with the ith user, and Δ_i the instantaneous AoI at the ith user. The instantaneous Δ_i is obtained from 41 to 44 based on the transmission mode. The indicator variable $l_i(t)$ is the respective average BLER derived in the previous section, since it represents the packet delivery probability in a given time slot.

B. RANDOM POLICY EWSAOI

The EWSAoI in (45) can be implemented directly using a random policy, where the base station (BS) randomly selects an action in each time slot. In the OMA mode, the BS randomly chooses which user to communicate with in a given time slot. For the NOMA, HD/FD cooperative SWIPT NOMA modes, the power allocation coefficients are adopted for each time slot, as summarized in Table II. This strategy results in the outcomes presented in Figures 4 and 5, with a detailed discussion provided in Section V.

C. OPTIMAL POLICY TO MINIMIZE THE EWSAOI

To achieve optimal AoI should be minimized. Therefore, our **Problem 1** is

$$\begin{aligned} \min_{\pi} \quad & \overline{\Delta} \\ \text{s.t.} \quad & \alpha_{1t} + \alpha_{2t} = 1 \\ & 0 \leq \alpha_{it} < 1, \\ & 0 \leq b_{it} < 1, \\ & 0 \leq P < P_{\text{total}}, \end{aligned} \tag{46}$$

where π represents the sequence of actions at each time slot, α_{it} denotes the power allocated to user UE_i in timeslot t, while b_{it} is the power splitting factor to user UE_i in timeslot t, and P_{total} is the BS's maximum transmit power.

It is a common practice to set a maximum AoI to D, beyond which the utility of the status update becomes zero [39]. This approach quantifies the utility of the updates and facilitates modeling the system as a finite state system. Once the AoI exceeds this threshold, the packet is discarded, and a new packet is transmitted from the BS. Therefore, the instantaneous AoI in the OMA mode is modified as follows

$$\Delta_i(t+1) = \begin{cases} 1, & 1-\overline{\varepsilon}_i, \\ \min(\Delta_i(t)+1, \text{D}), & \overline{\varepsilon}_i, \end{cases} \tag{47}$$

and

$$\Delta_i(t+1) = \min(\Delta_i(t)+1, \text{D}). \tag{48}$$

The instantaneous AoI for the other modes is modified in a similar approach used for the OMA mode by setting maximum AoI and the respective average BLER to signify the indicator variable.

Next, we model the system as a finite state MDP problem to adaptively select the best transmission mode in a given time slot as follows. The AoI of the users in the next time slot is associated with the error probability obtained through the average BLER. The BS allocates the optimal power splitting coefficient, b , and the power allocation factors α_1, α_2 for the HD and FD modes. For the NOMA mode, the BS allocates the power allocation factors, while for the OMA mode the BS selects the optimal user to serve.

To model a practical system, we model the coefficients b and α as discrete from the following set [10].

$$\left\{\frac{1}{2K_1}, \frac{2}{2K_1}, \ldots \frac{1}{2} - \frac{1}{2K_1}\right\} \text{and} \left\{\frac{1}{K_2}, \frac{2}{K_2}, \ldots 1 - \frac{1}{K_2}\right\}, \tag{49}$$

where $K_1 \geq 2$, and $K_2 \geq 2$.

We now formulate a policy that minimizes the EWSAoI summarized in 46, as follows. A finite state MDP is described by tuple $\{\mathcal{S}, \mathcal{A}, P, r\}$ with the State space $\mathcal{S}$, action space $\mathcal{A}$, Transitional probabilities P, and reward r as follows.

Let the state space S, be defined as $\{A_t, B_t, \Delta_{1t}, \Delta_{2t}\}$ such that, the state s_t at time slot t comprises the instantaneous AoI of both users Δ_{1t}, Δ_{2t}, and the indicators A_t and B_t. Here, A_t indicates the scenario where the BS can initiate a new action in this state. If $A_t = 0$, the BS can select a new action while $A_t \neq 0$, the BS cannot choose a new action in this state. Additionally, $A_t \neq 0$ implies that the state is in the second phase of HD mode. The value of A_t is the power allocation of the previous state under the HD mode. Moreover, $B_t = 1$ signifies that the state is in the second phase of HD mode, and UE_1 has successfully decoded x_2 in the first phase while $B_t = 0$, denotes other states.

The action space is defined by the policy π comprising a finite series of actions at each time slot, represented by $\{a_t\}$, for the four transmission modes paired with their respective power allocations and the energy harvesting coefficients. We adopted an action coding strategy to streamline the action representation [11] for all discrete coefficients in 49. However, our analysis includes more actions due to adding the FD mode to the system.

$$a_t \in \{1 \sim (K_1+1)(K_2+1)+2\}, \tag{50}$$

where $K_1 = K_2 = 5$.

- If $a_t \in \{1 \sim (K_1-1)(K_2-1)\}$, the BS selects the FD Cooperative-SWIPT-NOMA scheme.
- For $a_t \in \{1 \sim (K_1-1)(K_2-1)+1 \sim (K_1+1)(K_2)+2\}$, the HD Cooperative-SWIPT-NOMA scheme is chosen. where, $\alpha_1 = \frac{((a_t-1) \mod (K_1-1)+1)}{2K_1}$ and $b = \frac{(\lfloor (a_t-1)/(K_1-1) \rfloor +1)}{K_2}$ for cooperative schemes.
- If $a_t \in \{1 \sim (K_1+1)(K_2)+3 \sim (K_1+1)(K_2+1)\}$, the BS opts for the NOMA scheme and $\alpha_1 = \frac{(a_t-(K_1-1)(K_2-1))}{2K_1}$, and $\alpha_2 = 1-\alpha_1$.
- Otherwise, if $a_t = (K_1+1)(K_2+1)+1$ or $a_t = (K_1+1)(K_2+1)+2$, the OMA scheme is selected for transmission to UE_1 and UE_2, respectively.

where "mod" represents the remainder operator, and $\lfloor \cdot \rfloor$ denotes the round down operator.

The transition probability **P**: $P(s_{t+1}|s_t, a_t)$ is the probability of transitioning from state s_t to next state s_{t+1} through taking an action a_t.

If $A_t = 0$ and $a_t \in \{1 \sim (K_1-1)(K_2-1)\}$, the BS chooses the FD mode with the following transitions

$$s_{t+1} = \begin{cases} (a_t, B_t = 0, \Delta_{1t}+1, 1), & \overline{\varepsilon}_1^{\text{F}}(a_t)(1-\overline{\varepsilon}_2^{\text{F}}(a_t)), \\ (a_t, B_t = 0, 1, \Delta_{2t}+1), & (1-\overline{\varepsilon}_1^{\text{F}}(a_t))\overline{\varepsilon}_2^{\text{F}}(a_t), \\ (a_t, B_t = 0, \Delta_{1t}+1, \Delta_{2t}+1), & \overline{\varepsilon}_1^{\text{F}}(a_t)\overline{\varepsilon}_2^{\text{F}}(a_t), \\ (a_t, B_t = 1, 1, 1), & (1-\overline{\varepsilon}_1^{\text{F}}(a_t))(1-\overline{\varepsilon}_2^{\text{F}}(a_t)). \end{cases} \tag{51}$$

If $A_t = 0$, $a_t \in \{1 \sim (K_1-1)(K_2-1)+1 \sim (K_1+1)(K_2)+2\}$, the BS chooses HD mode with the following transitions

$$s_{t+1} = \begin{cases} (a_t, B_t = 0, \Delta_{1t}+1, \Delta_{2t}+1), & \overline{\varepsilon}_{12}^{\text{H}}(a_t), \\ (a_t, B_t = 1, \Delta_{1t}+1, \Delta_{2t}+1), & \\ \overline{\varepsilon}_{11}^{\text{H}}(a_t) - \{\overline{\varepsilon}_{11}^{\text{H}}(a_t), \overline{\varepsilon}_{12}^{\text{H}}(a_t)\}, & \\ (a_t, B_t = 1, 1, \Delta_{2t}+1), & 1-\overline{\varepsilon}_1^{\text{H}}(a_t). \end{cases} \tag{52}$$

If $A_t = 0, a_t \in \{1 \sim (K_1+1)(K_2)+3 \sim (K_1+1)(K_2+$

$1)\}$, the BS chooses NOMA for transmission to the UE_s

$$s_{t+1}=\begin{cases}(a_t, B_t=0, \Delta_{1t}+1, 1), & \bar{\varepsilon}_1^{\mathrm{N}}(a_t)(1-\bar{\varepsilon}_2^{\mathrm{N}}(a_t)),\\ (a_t, B_t=0, 1, \Delta_{2t}+1), & (1-\bar{\varepsilon}_1^{\mathrm{N}}(a_t))\bar{\varepsilon}_2^{\mathrm{N}}(a_t),\\ (a_t, B_t=0, \Delta_{1t}+1, \Delta_{2t}+1), & \bar{\varepsilon}_1^{\mathrm{N}}(a_t)\bar{\varepsilon}_2^{\mathrm{N}}(a_t),\\ (a_t, B_t=1, 1, 1), & (1-\bar{\varepsilon}_1^{\mathrm{N}}(a_t))(1-\bar{\varepsilon}_2^{\mathrm{N}}(a_t)).\end{cases} \tag{53}$$

If $A_t=0$, $a_t=(K_1+1)(K_2+1)+1$, the BS chooses OMA and transmission to UE_1

$$s_{t+1}=\begin{cases}(a_t, B_t=0, \Delta_{1t}+1, \Delta_{2t}+1), & \bar{\varepsilon}_1^{\mathrm{O}}(a_t),\\ (a_t, B_t=0, 1, \Delta_{2t}+1), & 1-\bar{\varepsilon}_1^{\mathrm{O}}(a_t).\end{cases} \tag{54}$$

If $A_t=0$, $a_t=(K_1+1)(K_2+1)+2$, the BS chooses OMA and transmission to UE_2

$$s_{t+1}=\begin{cases}(a_t, B_t=0, \Delta_{1t}+1, \Delta_{2t}+1), & \bar{\varepsilon}_2^{\mathrm{O}}(a_t),\\ (a_t, B_t=0, \Delta_{2t}+1, 1), & 1-\bar{\varepsilon}_2^{\mathrm{O}}(a_t).\end{cases} \tag{55}$$

If $A_t=a_{t-1}\neq 0$, this state s_t is in the second phase of HD Cooperative-SWIPT-NOMA, and the state transition probability is related to A_t, that is, a_{t-1}. When $B_t=1$,

$$s_{t+1}=\begin{cases}(0, B_t=1, \Delta_{1t}+1, \Delta_{2t}+1), & \bar{\varepsilon}_{23}^{\mathrm{H}}(a_t),\\ (0, B_t=1, \Delta_{1t}+1, 2), & 1-\bar{\varepsilon}_{23}^{\mathrm{H}}(a_t).\end{cases} \tag{56}$$

When $B_t=0$,

$$s_{t+1}=\begin{cases}(0, B_t=0, \Delta_{1t}+1, \Delta_{2t}+1), & \bar{\varepsilon}_{22}(a_t),\\ (0, B_t=0, \Delta_{1t}+1, 2), & 1-\bar{\varepsilon}_{22}(a_t).\end{cases} \tag{57}$$

The reward r is defined in terms of state and action pairs by $r(s_t,a_t)=w_1\Delta_{1,t}+w_2\Delta_{2,t}$. Starting from the initial state $s_0=\{0,0,1,1\}$ the long-term average reward under policy π is expressed as.

$$C(\pi,s_0)=\lim_{T\to\infty}\sup\frac{1}{T}\sum_{t=0}^{T}\mathbb{E}^{\pi}[r(s_t,a_t)|s_0]. \tag{58}$$

Therefore Problem 1 can be rewritten as

Problem 2.

$$\min_{\pi} C(\pi,s_0). \tag{59}$$

Before solving 58, we prove the existence of a time-invariant and deterministic policy for every action through the following theorem. *Proof*: See Appendix C

Theorem 1. An optimal policy π^*, to minimize the total average cost is obtained by solving the Bellman optimality equation with an optimal average return I^* and value function $V(s)$.

$$I^*+V(s)=\min_{a\in\mathcal{A}}\{r(s,a)+\mathbb{E}[V(\hat{s})|s,a]\}, \forall_s\in\mathcal{S}, \tag{62}$$

where π^* is the optimal policy, I^* is the optimal average return, $V(s)$ is the value function of state s, $r(s,a)$ is the immediate cost incurred by taking action a in state s, $\mathcal{A}$ is the set of all possible actions, $\mathcal{S}$ is the set of all possible states, $\hat{s}$ denotes the next state resulting from action a in state s, $\mathbb{E}[V(\hat{s}) \mid s,a]$ is the expected value function over the next state given current state and action.

Algorithm 1 To solve the Dynamic Programming Algorithm

Input: MDP parameters: State space $\mathcal{S}$, action space $\mathcal{A}$, Transitional probabilities P, reward r, Total time horizon $T=10^6$, $K_1=K_2=5$.

Output: EWSAoI, $\overline{\Delta}$.

1: Set initial state, $\{A,B,\Delta_1,\Delta_2\}=\{0,0,1,1\}$
2: Action space $\mathcal{A}\in\{1\sim(K_1+1)(K_2+1)+2\}$
3: Set $t=T, V_{s_t}^*=1, r(s_t,a_t,s_{t+1})$ for all t
4: **for** $t=T:-1:1$ **do**
5: **for** $s_t\in\mathcal{S}$ **do**
6: Compute Optimal policy $\pi^*(s_t)$

$$\pi^*(s_t)=\arg\min_{a_t\in A}\sum_{s_{t+1}\in\mathcal{S}}P(s_{t+1}|s_t,a_t)\left[r(s_t,a_t,s_{t+1})+V_{s_{t+1}}^*\right] \tag{60}$$

7: **end for**
8: **for** $s_t\in\mathcal{S}$ **do**
9: Compute Optimal value $V_{s_t}^*$

$$V_{s_t}^*=\min_{a_t\in\mathcal{A}}\left\{r(s_t,a_t,s_{t+1})+\sum_{s_{t+1}\in\mathcal{S}}P(s_{t+1}|s_t,a_t)V_{s_{t+1}}^*\right\} \tag{61}$$

10: **end for**
11: **end for**
12: Calculate the EWSAoI, $\overline{\Delta}$ according to (45).

$\hat{s}$ denotes the next state resulting from action a in state s, $\mathbb{E}[V(\hat{s}) \mid s,a]$ is the expected value function over the next state given current state and action.

The MDP formulation defines a finite state space based on the AoI for two users, $(\Delta_{1t},\Delta_{2t})$, and mode indicators (A_t,B_t), resulting in a manageable state space for small-scale systems. However, for N users, the state space grows exponentially as $O(D^N)$, where D is the maximum AoI, making the Bellman optimality equation (62) computationally intensive due to the need to evaluate all state-action pairs. To address this for massive UEs, heuristic or approximate dynamic programming methods, such as value function approximation or reinforcement learning, can be employed to reduce complexity while maintaining near-optimal performance. The MDP formulation is summarized further in the algorithm 1

D. SUB-OPTIMAL POLICY TO MINIMIZE THE EWSAOI

To reduce the computational complexity associated with the MDP, a sub optimal policy based on the DPP strategy for Lyapunov optimization is proposed. Lyapunov drift-plus-penalty techniques have been widely applied in time analysis to optimize resource allocation and ensure stability in dynamic wireless systems [40]. The policy does not rely on any statistical underlying process for decision-making. According to the Lyapunov theorem, a control strategy should minimize the Lyapunov function at each timeslot and for improvement, substitute a constraint for the conditional Lyapunov drift [41]. The Lyapunov function of the queue vector $Q(t)$ is given as

Algorithm 2 To solve the Drift-Plus-Penalty Algorithm

Input: Total time horizon, $T = 10^6$, $K_1 = K_2 = 5$.

Output: EWSAoI, $\bar{\Delta}$.

1: Set initial state, $\{A, B, \Delta_1, \Delta_2\} = \{0, 0, 1, 1\}$
2: **for** $t = 1 \longrightarrow T$ **do**
3: **for** $a_t = 1 \longrightarrow (K_1 + 1)(K_2 + 1) + 2$ **do**
4: Obtain the Lyapunov drift as (65) per and (66).
5: **end for**
6: Choose the action $\min_{a_t} \left[\Phi^{\mathrm{N,O,F}}(\Delta(\vec{t})), \Phi^{\mathrm{H}}(\Delta(\vec{t}))\right]$.
7: Update the states according $\{A, B, \Delta_1, \Delta_2\}$ according to the selected action based on (41)-(44).
8: **end for**
9: Calculate the EWSAoI, $\bar{\Delta}$ according to (45).

follows:

$$L(Q(t)) = \frac{1}{2}\sum_{i=1}^{N} Q_i^2(t). \tag{63}$$

The Lyapunov drift equation offers such a constraint as.

$$\Delta(Q(t)) = \mathbb{E}\{L(Q(t+1)) - L(Q(t))|Q(t)\}. \tag{64}$$

The structure of the Lyapunov drift equation for the FD mode mirrors that of the OMA and NOMA modes, as all three complete the transmission within a single time slot. Consequently, the Lyapunov drift expressions for the OMA, NOMA, and FD modes are derived similarly, following the approach in [11].

$$\Phi^{\mathrm{N,O,F}}(\Delta(\vec{t})) = -\frac{1}{N}\sum_{i=1}^{N}(1 - \bar{\varepsilon}_i(a_t)w_i\Delta_i(t)) + \frac{1}{N}\sum_{i=1}^{N} w_i \tag{65}$$

And the two-slot Lyapunov drift for HD Cooperative SWIPT NOMA as

$$\Phi^{\mathrm{H}}(\Delta(\vec{t})) = -\frac{1}{2N}\sum_{i=1}^{N}(1 - \bar{\varepsilon}_C(a_t)w_i\Delta_i(t)) + \frac{1}{N}\sum_{i=1}^{N} w_i. \tag{66}$$

Therefore, in the current state s_t, if $A_t = 0$, the policy chooses action a_t from action space A_t with the minimum value of $\min_{a_t} \left[\Phi^{\mathrm{N,O,F}}(\Delta(\vec{t})), \Phi^{\mathrm{H}}(\Delta(\vec{t}))\right]$; if $A_t = a_{t-1} \neq 0$, the policy cannot select a new action.

The Drift-Plus-Penalty (DPP) algorithm (Algorithm 2) achieves linear complexity concerning the number of users, $O(N)$, as the Lyapunov function (Equation 60) scales with the sum of squared AoI values, making it more scalable than the MDP's exponential complexity, $O(D^N)$. However, for massive user equipment (UE) scenarios, the action space grows with power allocation and mode combinations, potentially necessitating user clustering to group UEs with similar channel conditions, thereby reducing computational overhead while maintaining effective AoI minimization.The above DPP formulation is further summarized in algorithm 2

TABLE 2. Simulation parameters.

Parameter	Value
Random policy NOMA power allocation coefficients	α_1= 0.2, α_2= 0.8
Random policy power splitting coefficient	$\mathrm{b} = 0.3$
Pathloss exponent	$\phi = 3$
CDF parameters $\mathrm{m}, \mathrm{n}, \mathrm{v}$	$1.8, 2, 1.2$
Maximum AoI	Δ_{max}=100
Time horizon	$\mathrm{T} = 10^6$
Parameters K_1, K_2	5
Number of bits, blocklength	N=80, m=100

V. SIMULATION RESULTS

In this section, we interpret and discuss the results from our proposed model, emphasizing the significance of BLER and the necessity of extending our analysis to the AoI. The simulation Table II outlines the parameters used for the random policy, along with general settings. The parameters for the MDP, and the DPP policies are optimally selected within the algorithms described in section IV.

A. AVERAGE BLER OF THE TRANSMISSION SCHEMES

First, we validate the analytical framework through Monte Carlo simulations. In Fig. 2, the results show that the average BLER obtained from the analytical framework and the Monte Carlo simulations are tight, confirming the accuracy of our error performance analysis. Validation for the OMA and NOMA modes is omitted, as the equations used are the same as the HD mode. Additionally, the HD mode incorporates our new ideas, such as receiver diversity in the direct phase and transmit beamforming in the cooperative phase.

Fig. 3 shows the average BLER for each user and mode. The dashed line plots represent the distance configuration $d_1 = 1, d_2 = 3, d_3 = 2$ while the solid lines represent the distance configuration $d_1 = 2, d_2 = 3, d_3 = 1$. Overall, the HD mode provides the best average BLER for both users, while the OMA mode provides the best average BLER in isolation. Furthermore, in the higher transmit SNR region UE_2 has a better average BLER compared to UE_1 as shown by the curve crossing of the FD and HD modes.

The average BLER is a good metric to quantify reliability, such as the order 10^{-5} required for crucial URLLC requirements [42] and 10^{-9} for mission-critical applications. However, as demonstrated in Fig. 3 this not easily achieved even at high SINR. Additionally, monitoring and control applications in a multi-user scenario require scheduling to select the best transmission, which the user's average BLER does not directly demonstrate. Therefore, based on the average BLER the AoI is evaluated at all the operating modes because it quantifies both latency and inter-delivery time of the packets.

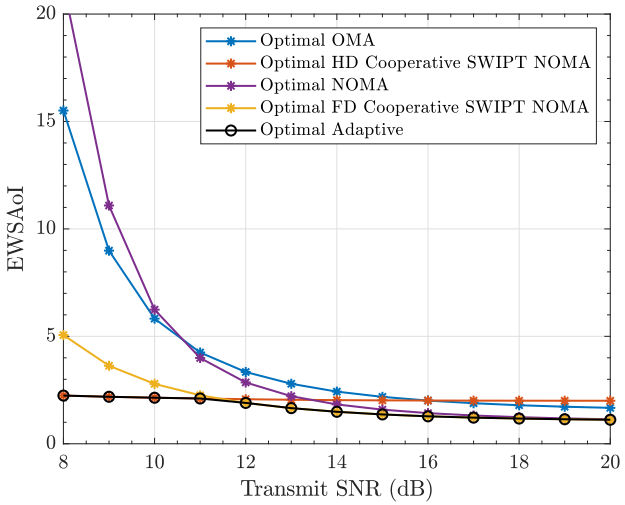

FIGURE 6. Optimal Policy EWSAoI versus SNR at (d_1=1, d_2=3, d_3=2).

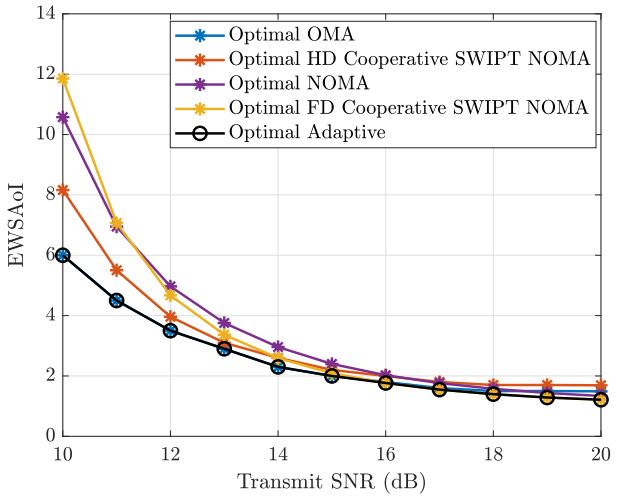

FIGURE 7. Optimal Policy EWSAoI versus SNR at (d_1=2, d_2=3, d_3=1).

B. AOI ANALYSIS FOR THE TRANSMISSION SCHEMES

The EWSAoI for two distance configurations is plotted in closed-form from (45) to obtain Fig. 4 and Fig. 5. The results obtained through a random policy show that different schemes exhibit performance advantages depending on the distance configurations. For instance, NOMA is the best mode for high transmit SNR, while the proposed HD mode is the best for low transmit SNR at a shorter distance below 1.5 between the BS and UE_1. The OMA scheme is always better at large distances and low transmit SNR. This is the basis for the optimal and suboptimal strategies described in Section IV.

Fig. 6 and Fig. 7 show that the optimal decision enables the operation at lower SNR for both distance configurations. Furthermore, the results show that selecting the optimal powers in the NOMA-based modes and the optimal user to serve for the OMA mode provide a lower AoI than the random policy results. At distance configuration $d_1 = 1, d_2 = 3, d_3 = 1$, the proposed HD mode has the lowest AoI at low transmit SNR. Additionally, this proposed HD mode maintains a good performance at $d_1 = 2, d_2 = 3, d_3 = 1$ against the OMA mode, which is ideal for this configuration, while at the same time outperforms the FD and NOMA modes. This improved performance of the HD mode is attributed to the receive diversity introduced in the direct phase at UE_1 and the transmit beamforming in the cooperative phase that maintains a good error performance for both configurations. The NOMA scheme provides the best AoI performance in the high transmit SNR region for all distance configurations. This is attributed to the successful packet delivery to both users within the same time slot without requiring two phases in the cooperative modes. Furthermore, the optimal adaptive policy selects the best strategy in every time slot, hence providing the lowest possible setting of the AoI in each distance configuration. Finally, Fig. 8 shows that the suboptimal based on the drift plus penalty policy approach provides near-optimal results while providing lower complexity. This is obtained by selecting the action that minimises Lyapunov drift. This approach reduces both the computation overhead of the MDP and the deployment complexity in resource-constrained environments like IoT devices.

VI. CONCLUSION

In this work, we considered the AoI minimization problem in an adaptive OMA, NOMA, FD/HD cooperative SWIPT NOMA system. Specifically, we introduced the idea of receiver diversity when UE_1 is not operating in FD mode and further propose transmit BF for the HD scheme in the cooperative phase to fully exploit both antennas on UE_1 used for full duplex operation. Consequently, we developed an analytical framework by deriving average BLER closed-form expressions while validating them through Monte Carlo sim-

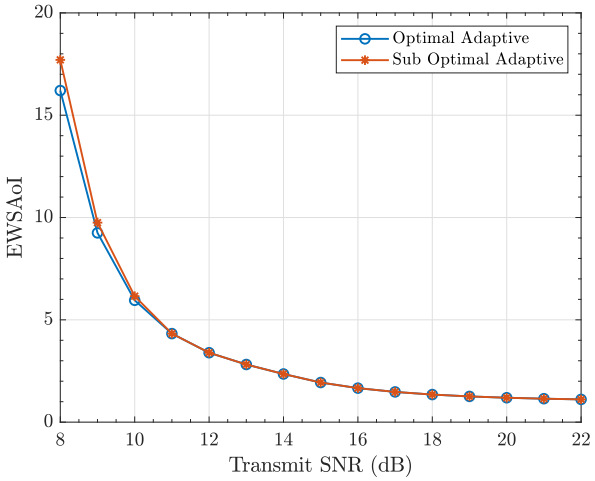

FIGURE 8. Optimal and Sub Optimal Policy EWSAoI versus SNR at (d_1=2, d_2=3, d_3=1).

ulations. Based on the obtained results, the scheme-wise AoI is analyzed, demonstrating a configuration-dependent performance of the different schemes. To exploit these performance advantages of each scheme, we suggested an adaptive policy leveraging the MDP and a lower complexity policy based on the drift plus penalty algorithm. The results show that the proposed approach minimizes AoI in wireless networks and offers insights into practical system design. Future work will investigate multi-user NOMA with user clustering and distributed optimization to address scalability in massive UE scenarios. By grouping UEs based on channel conditions, clustering can reduce the action space complexity, while distributed optimization enables local decision-making at each UE, mitigating the computational burden of centralized MDP and DPP approaches. These strategies aim to maintain low AoI in large-scale systems while managing multi-user interference effectively.

APPENDIX

A. AVERAGE BLER EQUATION

Proof.

$$\bar{\varepsilon}_{i,j} = \int_0^{\infty} Z(\gamma_{i,j}) f_{\gamma_{i,j}}(x)\, dx$$

Substituting for $Z(\gamma_{i,j})$ in (27) and (28)

$$= \int_0^{v_i} f_{\gamma_{i,j}}(x)\, dx + \int_{v_i}^{u_i} \left(\frac{1}{2} - \omega_i(x-\Omega)\right) f_{\gamma_{i,j}}(x)\, dx$$

$$= \frac{1}{2}\left(F_{\gamma_{i,j}}(u_i) + F_{\gamma_{i,j}}(v_i)\right) + \omega\Omega(F_{\gamma_{i,j}}(u_i) - F_{\gamma_{i,j}}(v_i)) - \omega \int_{v_i}^{u_i} x f_{\gamma_{i,j}}(x)\, dx.$$

Using integration by parts yields

$$= \frac{1}{2}(F_{\gamma_{i,j}}(v_i) + F_{\gamma_{i,j}}(u_i)) + \omega\Omega(F_{\gamma_{i,j}}(u_i) - F_{\gamma_{i,j}}(v_i)) - (\omega(u_i F_{\gamma_{i,j}}(u_i) - v_i F_{\gamma_{i,j}}(v_i)) + \omega \int_{v_i}^{u_i} F_{\gamma_{i,j}}(x)\, dx$$

substituting for u and v

$$= \frac{1}{2}\left(F_{\gamma_{i,j}}(v_i) + F_{\gamma_{i,j}}(u_i)\right) + \omega\Omega(F_{\gamma_{i,j}}(u_i) - F_{\gamma_{i,j}}(v_i)) - (\omega\left(\Omega + \frac{1}{2\omega}\right) F_{\gamma_{i,j}}(u_i) - \omega\left(\Omega - \frac{1}{2\omega}\right) F_{\gamma_{i,j}}(v_i)) + \omega \int_{v_i}^{u_i} F_{\gamma_{i,j}}(x)\, dx$$

$$= \omega \int_{v_i}^{u_i} F_{\gamma_{i,j}}(x)\, dx$$

□

B. STATIONARY AND DETERMINISTIC POLICY

Proof. In [11], [43], the conditions for the existence of an average optimal policy are stated as follows:

There exists a positive constant $\delta < 1$, Q, and q, and a measurable function $\omega \geq 1$ on S, where $s = A, B, \Delta_1, \Delta_2$, such that the reward function $|r(s,a)| \leq Q\omega(s)$ for all state-action pairs (s,a) and

$$\sum_{\hat{s}\in S} \omega(\hat{s}) P(\hat{s}|s,a) \leq \delta\omega(s) + q. \tag{67}$$

Therefore, when $\omega(s) = w_1\Delta_1 + w_2\Delta_2$ and $q > w_1 + w_2$, if $A = 0$, there exists

$$\max_a \left\{ \frac{w_1\Delta_1\bar{\varepsilon}_1^{\mathrm{H}}(a) + w_2\Delta_2 + 1 - q}{w_1\Delta_1 + w_2\Delta_2}, \frac{w_1\Delta_1\bar{\varepsilon}_1^{\mathrm{O}} + w_2\Delta_2 + 1 - q}{w_1\Delta_1 + w_2\Delta_2}, \frac{w_1\Delta_1 + w_2\Delta_2\bar{\varepsilon}_2^{\mathrm{O}} + 1 - q}{w_1\Delta_1 + w_2\Delta_2}, \frac{w_1\Delta_1\bar{\varepsilon}_1^{\mathrm{F}}(a) + w_2\Delta_2\bar{\varepsilon}_2^{\mathrm{F}}(a) + 1 - q}{w_1\Delta_1 + w_2\Delta_2}, \frac{w_1\Delta_1\bar{\varepsilon}_1^{\mathrm{N}}(a) + w_2\Delta_2\bar{\varepsilon}_2^{\mathrm{N}}(a) + 1 - q}{w_1\Delta_1 + w_2\Delta_2} \right\} \leq \delta < 1$$

that meets the condition. If $A \neq 0$ and $B = 1$, there exists

$$\frac{w_1\Delta_1 + w_2(\Delta_2 - 1) + 1)\bar{\varepsilon}_2^{23}(a) + 1 - q}{w_1\Delta_1 + w_2\Delta_2} \leq \delta < 1$$

that meets the condition. Similarly, if $A \neq 0$ and $B = 0$, there exists

$$\frac{w_1\Delta_1 + w_2(\Delta_2 - 1) + 1)\bar{\varepsilon}_2^{22}(a) + 1 - q}{w_1\Delta_1 + w_2\Delta_2} \leq \delta < 1$$

that meets the condition.

Furthermore, there exist two value functions $v_1, v_2 \in B_\omega(S)$ and some state $s_0 \in S$, such that

$$v_1(s) \leq h_\lambda(s) \leq v_2(s), \quad \text{for all } s \in S \text{ and } \lambda \in (0,1), \tag{68}$$

where $h_\lambda(s) = V_\lambda(s) - V_\lambda(s_0)$ and $B_\omega(S) := \{u : |u|\omega < \infty\}$ denotes the Banach space, $|u|\omega := \sup_{s\in S} \omega(s)^{-1}|u(s)|$ denotes the weighted supremum norm.

According to condition 1, we show that there exists $\frac{w_1\Delta_1 + w_2\Delta_2 + w_1 + w_2}{w_1\Delta_1 + w_2\Delta_2} \leq \kappa < \infty$ such that

$$\sum_{\hat{s}\in S} \omega(\hat{s}) P(\hat{s}|s,a) \leq \kappa\omega(s) \tag{69}$$

for all (s,a), and for $d \in D^{MD}$, where D^{MD} denotes the set of Markovian and deterministic (MD) decision rules. We can derive that

$$\sum_{\hat{s}\in S} \omega(\hat{s}) P_d(\hat{s}|s,a) \leq \omega(s) + w_1 + w_2 \leq (1+1)\omega(s), \tag{70}$$

so that, for each λ, $0 \leq \lambda < 1$, there exists an integer Z such that

$$\lambda^Z \sum_{\hat{s}\in S} \omega(\hat{s}) P_{\pi^Z}(\hat{s}|s,a) \leq \lambda^Z(\omega(s) + Z) < \lambda^Z(1+Z)\omega(s), \tag{71}$$

where $\pi = (d_1, \ldots, d_N)$, $d_i \in D^{MD}$, $1 \leq i \leq Z$. Then, according to Proposition 6.10.1 in [44], for each $\pi \in D_{MD}$, there exists a θ, $0 \leq \theta < 1$, such that the value function satisfies

$$|V_\lambda^\pi(s)| \leq \frac{1}{1-\theta}[1 + \lambda\kappa + \ldots + (\lambda\kappa)^{(Z-1)}]\omega(s). \tag{72}$$

□

References

[1] B. Uwizeyimana, M. Abo-Zahhad, O. Muta, *et al.*, "Joint user association and pairing in multi-UAV-assisted NOMA networks: A decaying-epsilon thompson sampling framework," *IEEE Access*, 2024.

[2] L. B. Luat, N. C. Luong, and D. I. Kim, "Integrated radar and communication in ultra-reliable and low-latency communications-enabled uav networks," *IEEE Transactions on Vehicular Technology*, 2025.

[3] Y. Liu, X. Wang, G. Zheng, *et al.*, "An AoI-aware data transmission algorithm in blockchain-based intelligent healthcare systems," *IEEE Transactions on Consumer Electronics*, 2024.

[4] M. A. Abd-Elmagid, N. Pappas, and H. S. Dhillon, "On the role of age of information in the internet of things," *IEEE Communications Magazine*, vol. 57, no. 12, pp. 72–77, 2019.

[5] S. Kaul, R. Yates, and M. Gruteser, "Real-time status: How often should one update?" In *2012 Proceedings IEEE INFOCOM*, IEEE, 2012, pp. 2731–2735.

[6] I. Kadota, A. Sinha, E. Uysal-Biyikoglu, *et al.*, "Scheduling policies for minimizing age of information in broadcast wireless networks," *IEEE/ACM Transactions on Networking*, vol. 26, no. 6, pp. 2637–2650, 2018.

[7] A. M. Bedewy, Y. Sun, and N. B. Shroff, "Minimizing the age of information through queues," *IEEE Transactions on Information Theory*, vol. 65, no. 8, pp. 5215–5232, 2019.

[8] A. Maatouk, M. Assaad, and A. Ephremides, "Minimizing the age of information: NOMA or OMA?" In *IEEE INFOCOM 2019-IEEE Conference on Computer Communications Workshops (INFOCOM WKSHPS)*, IEEE, 2019, pp. 102–108.

[9] Y. Polyanskiy, H. V. Poor, and S. Verdú, "Channel coding rate in the finite blocklength regime," *IEEE Transactions on Information Theory*, vol. 56, no. 5, pp. 2307–2359, 2010.

[10] Q. Wang, H. Chen, Y. Li, and B. Vucetic, "Minimizing age of information via hybrid NOMA/OMA," in *2020 IEEE International Symposium on Information Theory (ISIT)*, IEEE, 2020, pp. 1753–1758.

[11] S. Wu, C. Guo, Z. Deng, *et al.*, "Optimizing age of information in adaptive NOMA/OMA/cooperative-SWIPT-NOMA system," *IEEE Transactions on Wireless Communications*, vol. 21, no. 12, pp. 11 125–11 138, 2022.

[12] S. Kaboyo, A. H. Abd El-Malek, O. Muta, *et al.*, "Age of information analysis for full duplex cooperative swipt noma system," in *2024 IEEE Wireless Communications and Networking Conference (WCNC)*, IEEE, 2024, pp. 1–6.

[13] Z. Ding, M. Peng, and H. V. Poor, "Cooperative non-orthogonal multiple access in 5G systems," *IEEE Communications Letters*, vol. 19, no. 8, pp. 1462–1465, 2015.

[14] Y. Liu, Z. Ding, M. Eıkashlan, and H. V. Poor, "Cooperative non-orthogonal multiple access in 5G systems with SWIPT," in *2015 23rd European signal processing conference (EUSIPCO)*, IEEE, 2015, pp. 1999–2003.

[15] A. A. Hamza, I. Dayoub, I. Alouani, and A. Amrouche, "On the error rate performance of full-duplex cooperative NOMA in wireless networks," *IEEE Transactions on Communications*, vol. 70, no. 3, pp. 1742–1758, 2021.

[16] A. Baranwal, S. Sharma, S. D. Roy, and S. Kundu, "On performance of a full duplex SWIPT enabled cooperative NOMA network," *Wireless Networks*, pp. 1–14, 2023.

[17] I. S. Gradshteyn and I. M. Ryzhik, *Table of integrals, series, and products*. Academic press, 2014.

[18] T. M. Hoang, B. C. Nguyen, X. N. Tran, T. Kim, *et al.*, "Secrecy performance analysis for mimo-df relay systems with mrt/mrc and tzf/mrc schemes," *IEEE Transactions on Vehicular Technology*, vol. 72, no. 8, pp. 10 173–10 186, 2023.

[19] F. Chai, Q. Zhang, H. Yao, *et al.*, "A hybrid noma-oma framework for multi-user offloading in mobile edge computing system," *IEEE Transactions on Services Computing*, 2025.

[20] X. Sun, S. Yan, N. Yang, *et al.*, "Short-packet downlink transmission with non-orthogonal multiple access," *IEEE Transactions on Wireless Communications*, vol. 17, no. 7, pp. 4550–4564, 2018.

[21] G. Durisi and H. Bölcskei, "High-snr capacity of wireless communication channels in the noncoherent setting: A primer," *AEU-International Journal of Electronics and Communications*, vol. 65, no. 8, pp. 707–712, 2011.

[22] X. Lai, Q. Zhang, and J. Qin, "Cooperative NOMA short-packet communications in flat rayleigh fading channels," *IEEE Transactions on Vehicular Technology*, vol. 68, no. 6, pp. 6182–6186, 2019.

[23] L. Yuan, Q. Du, and F. Fang, "Performance analysis of full-duplex cooperative NOMA short-packet communications," *IEEE Transactions on Vehicular Technology*, vol. 71, no. 12, pp. 13 409–13 414, 2022.

[24] X. Yue, Y. Liu, S. Kang, *et al.*, "Exploiting full/half-duplex user relaying in NOMA systems," *IEEE Transactions on Communications*, vol. 66, no. 2, pp. 560–575, 2017.

[25] M. Duarte, C. Dick, and A. Sabharwal, "Experiment-driven characterization of full-duplex wireless systems," *Trans. Wireless Commun*, vol. 11, no. 12, pp. 4296–4307, Dec. 2012.

[26] D.-T. Do, T.-L. Nguyen, S. Ekin, *et al.*, "Joint user grouping and decoding order in uplink/downlink MISO/SIMO-NOMA," *IEEE Access*, vol. 8, pp. 143 632–143 643, 2020.

[27] E. Björnson, M. Bengtsson, and B. Ottersten, "Optimal multiuser transmit beamforming: A difficult problem with a simple solution structure [lecture notes]," *IEEE Signal Processing Magazine*, vol. 31, no. 4, pp. 142–148, 2014.

[28] B. Makki, T. Svensson, and M. Zorzi, "Finite block-length analysis of the incremental redundancy HARQ," *Commun. Lett.*, vol. 3, no. 5, pp. 529–532, Oct. 2014.

[29] R. M. McLeod, *The generalized Riemann integral*. American Mathematical Soc., 1980, vol. 20.

[30] Y. Gu, H. Chen, Y. Li, and B. Vucetic, "Ultra-reliable short-packet communications: Half-duplex or full-duplex relaying?" *Wireless Commun. Lett.*, vol. 7, no. 3, pp. 348–351, Jun. 2017.

[31] A. Goldsmith, *Wireless communications*. Cambridge university press, 2005.

[32] T.-H. Vu, T.-V. Nguyen, Q.-V. Pham, *et al.*, "Hybrid long-and short-packet based NOMA systems with joint power allocation and beamforming design," *IEEE Transactions on Vehicular Technology*, vol. 72, no. 3, pp. 4079–4084, 2022.

[33] Y. Chen, G. K. Karagiannidis, H. Lu, and N. Cao, "Novel approximations to the statistics of products of independent random variables and their applications in wireless communications," *IEEE Transactions on Vehicular Technology*, vol. 61, no. 2, pp. 443–454, 2012. DOI: 10.1109/TVT.2011.2178441.

[34] M. D. Springer and W. E. Thompson, "The distribution of products of beta, gamma and gaussian random variables," *SIAM Journal on Applied Mathematics*, vol. 18, no. 4, pp. 721–737, 1970.

[35] D. L. Djukić, R. M. M. Djukić, L. Reichel, and M. M. Spalević, "Weighted averaged gaussian quadrature rules for modified chebyshev measures," *Applied Numerical Mathematics*, vol. 200, pp. 195–208, 2024.

[36] S. Kaul, M. Gruteser, V. Rai, and J. Kenney, "Minimizing age of information in vehicular networks," in *2011 8th Annual IEEE communications society conference on sensor, mesh and ad hoc communications and networks*, IEEE, 2011, pp. 350–358.

[37] G. Liu, X. Chen, Z. Ding, *et al.*, "Hybrid half-duplex/full-duplex cooperative non-orthogonal multiple access with transmit power adaptation," *Trans. Wireless Commun.*, vol. 17, no. 1, pp. 506–519, Jan. 2017.

[38] Y. Liu, Z. Ding, M. Elkashlan, and H. V. Poor, "Cooperative non-orthogonal multiple access with simultaneous wireless information and power transfer," *J. Sel. Areas Commun.*, vol. 34, no. 4, pp. 938–953, Apr. 2016.

[39] E. T. Ceran, D. Gündüz, and A. György, "A reinforcement learning approach to age of information in multi-user networks," in *2018 IEEE 29th Annual International Symposium on Personal, Indoor and Mobile Radio Communications (PIMRC)*, IEEE, 2018, pp. 1967–1971.

[40] N. Moghadam, H. Li, H. Zeng, and L. Liu, "Lyapunov scheduling and optimization in network coded wireless multicast network," *IEEE Transactions on Vehicular Technology*, vol. 67, no. 6, pp. 5135–5145, 2018.

[41] L. Bracciale and P. Loreti, "Lyapunov drift-plus-penalty optimization for queues with finite capacity," *IEEE Communications Letters*, vol. 24, no. 11, pp. 2555–2558, 2020.

[42] Y. Mao, O. Dizdar, B. Clerckx, *et al.*, "Rate-splitting multiple access: Fundamentals, survey, and future research trends," *IEEE Communications Surveys & Tutorials*, vol. 24, no. 4, pp. 2073–2126, 2022.

[43] X. Guo and Q. Zhu, "Average optimality for markov decision processes in borel spaces: A new condition and approach," *Journal of Applied Probability*, vol. 43, no. 2, pp. 318–334, 2006.

[44] M. L. Puterman, *Markov decision processes: discrete stochastic dynamic programming*. John Wiley & Sons, 2014.

SIMON KABOYO (Member, IEEE) received the B.Sc. degree in Telecommunications Engineering from Makerere University, Uganda in 2016. He received the M.Sc. in Electronics and Communication Engineering in 2024 at the Egypt Japan University of Science and Technology (E-JUST). He is currently a Ph.D student at McMaster University, Canada, in the Communication Research Lab. His research interests include Wireless Communication and Signal Processing, Information Freshness, and machine learning in communication systems. He previously served as a radio frequency optimization engineer on Huawei projects in Uganda, Botswana, Burundi, and Zambia.

MOHAMMED ABO-ZAHHAD (Senior Member, IEEE) received the B.S.E.E. and M.S.E.E. degrees in Electrical Engineering from Assiut University, Assiut, Egypt, in 1979 and 1983, respectively, and the dual Ph.D. degree from the University of Kent, Canterbury, U.K., and Assiut University (channel system), in 1988. He has been the Director of the AU Management Information System (MIS) Center and the Vice-Dean for graduated studies, Faculty of Engineering, Assiut University, since August 2006. He has also been a Professor in Electronics and Communication Engineering, since January 1999, the Dean of the School of Electronics, Communication and Computer Engineering, and a Professor in Communication and Electronics engineering with the Egypt-Japan University of Science and Technology (E-JUST), Alexandria, Egypt, since January 2017. He is currently the General Director of the E-JUST Information and Communication Technology Center, Alexandria. His research interests include switched capacitor, optical and digital filters, biomedical and genomic signal processing, speech processing, data compression, wavelet transforms, genetic algorithms, immune algorithms, wireless sensor networks, and electronic systems. He has published more than 160 papers in national and international journals and conferences in the above fields.

OSAMU MUTA (Member, IEEE) received an Associate B.E degree from Sasebo Institute of Technology in 1994, a B.E. degree from Ehime University, in 1996, an M.E. degree from Kyushu Institute of Technology in 1998, and a Ph.D. degree from Kyushu University in 2001. In 2001, he joined the Graduate School of Information Science and Electrical Engineering, Kyushu University as an assistant professor. During 2010-2023, he was an associate professor at the Center for Japan-Egypt Cooperation in Science and Technology, Kyushu University. Since 2023, he has been a professor at the Faculty of Information Science and Electrical Engineering, Kyushu University in Japan. His research interests include signal processing techniques for wireless communication and powerline communication, MIMO techniques, interference coordination techniques, low-power wide-area networks, and nonlinear distortion compensation techniques for high-power amplifiers. He is a Senior Member of the Institute of Electronics, Information, and Communication Engineering (IEICE). He was the recipient of the 2005 Active Research Award in IEICE Radio Communication Systems Technical Committee, the Chairperson's Award for Excellent Paper in IEICE Communication Systems Technical Committee (2014, 2015, and 2017), the 2020 IEICE Communications Society Best Paper Award, and the International Symposium on Computing and Networking 2022 (CANDAR'22) Best Paper Award, respectively.

AHMED H. ABD EL-MALEK (Senior Member, IEEE) received the B.Sc. and M.Sc. degrees in electrical engineering from Alexandria University, Egypt, in 2007 and 2010, respectively, and the Ph.D. degree from the Electrical Engineering Department, King Fahd University of Petroleum and Mineral (KFUPM), Saudi Arabia, in 2016. He is currently an Associate Professor with the Electronics and Communications Engineering Department, Egypt-Japan University of Science and Technology. His research interests include cognitive radio, design and analysis of wireless networks, network coding, physical layer security, and interference cancellation.

MAHA M. ELSABROUTY (Senior Member, IEEE) received the B.Sc. degree (Hons.) in Electrical, Electronics, and Communication Engineering from Cairo University, Egypt, and the M.Sc. and Ph.D. degrees in Electrical Engineering from the University of Ottawa. She is currently a Professor in wireless communications and signal processing with the Department of Electronics and Communications Engineering, Egypt-Japan University for Science and Technology (E-JUST) University. Her current research interests include massive MIMO techniques, interference management in HetNets, cognitive radio, intelligent techniques for wireless communications, and green communication systems.